NeuroImage 129 (2016) 247–259

Contents lists available at ScienceDirect

NeuroImage

journal homepage: www.elsevier.com/locate/ynimg

Statistical machine learning to identify traumatic brain injury (TBI) from structural disconnections of white matter networks

Jhimli Mitra [a,e,*], Kai-kai Shen [a], Soumya Ghose [a,e], Pierrick Bourgeat [a], Jurgen Fripp [a], Olivier Salvado [a], Kerstin Pannek [d], D. Jamie Taylor [c], Jane L. Mathias [b], Stephen Rose [a]

[a] CSIRO Health and Biosecurity, The Australian e-Health & Research Centre, Herston, QLD, Australia
[b] School of Psychology, University of Adelaide, Adelaide, SA, Australia
[c] Department of Radiology, The Royal Adelaide Hospital, Adelaide, SA, Australia
[d] Department of Computing, Imperial College London, London, United Kingdom
[e] Center for Computational Imaging and Personalized Diagnostics, Case Western Reserve University, Cleveland, OH, USA

ARTICLE INFO

Article history:
Received 18 February 2015
Accepted 24 January 2016
Available online 28 January 2016

Keywords:
Diffusion tractography
Structural network connections
Traumatic brain injury
Network-based statistics
Machine learning

ABSTRACT

Identifying diffuse axonal injury (DAI) in patients with traumatic brain injury (TBI) presenting with normal appearing radiological MRI presents a significant challenge. Neuroimaging methods such as diffusion MRI and probabilistic tractography, which probe the connectivity of neural networks, show significant promise. We present a machine learning approach to classify TBI participants primarily with mild traumatic brain injury (mTBI) based on altered structural connectivity patterns derived through the network based statistical analysis of structural connectomes generated from TBI and age-matched control groups. In this approach, higher order diffusion models were used to map white matter connections between 116 cortical and subcortical regions. Tracts between these regions were generated using probabilistic tracking and mean fractional anisotropy (FA) measures along these connections were encoded in the connectivity matrices. Network-based statistical analysis of the connectivity matrices was performed to identify the network differences between a representative subset of the two groups. The affected network connections provided the feature vectors for principal component analysis and subsequent classification by random forest. The validity of the approach was tested using data acquired from a total of 179 TBI patients and 146 controls participants. The analysis revealed altered connectivity within a number of intra- and inter-hemispheric white matter pathways associated with DAI, in consensus with existing literature. A mean classification accuracy of 68.16% ± 1.81% and mean sensitivity of 80.0% ± 2.36% were achieved in correctly classifying the TBI patients evaluated on the subset of the participants that was not used for the statistical analysis, in a 10-fold cross-validation framework. These results highlight the potential for statistical machine learning approaches applied to structural connectomes to identify patients with diffusive axonal injury.

Introduction

Traumatic brain injuries (TBIs) are highly heterogeneous, with injury resulting from a unique combination of mechanical forces that interact with each individuals distinctive neuroanatomy (Meaney and Smith, 2011). They are also dynamic, involving a complex cascade of metabolic events that affect important ionic fluxes, neurotransmitter concentrations, cerebral haemodynamic status, edema and neuro-inflammatory responses (Bigler and Maxwell, 2012; Taber and Hurley, 2013). Numerous studies indicate that a hallmark neuropathological feature of TBI is the presence of diffuse axonal injury (DAI) resulting from damage to axolemma and neuro-filaments within the brain (Bigler and Maxwell, 2012; Omalu et al., 2005). DAI is estimated to occur in approximately 40%–50% of all persons who sustain a TBI (Meythaler et al., 2001). The pathology of DAI has been investigated in some detail (Povlishock and Katz, 2005). If there is sufficient force to rupture the micro-vasculature, small hemorrhages or microbleeds may also be present, which are reliably detected using CT or MRI based susceptibility-weighted imaging (SWI) (Benson, 2012). Although CT and conventional MRI have been proven to be useful for the clinical management of moderate to severe TBI, conventional neuroimaging does not reliably detect DAI in cases of mild TBI (mTBI) (Hammoud and Wasserman, 2002; Iverson et al., 2000).

There is now growing evidence to suggest that diffusion tensor imaging (DTI) has the potential to revolutionize how we detect DAI in mTBI (Arfanakis et al., 2002; Bigler and Maxwell, 2012; Taber and Hurley, 2013; Niogi and Mukherjee, 2010; Shenton et al., 2012; Lipton

* Corresponding author at: CSIRO Health and Biosecurity, The Australian e-Health & Research Centre, Herston, QLD, Australia (past affiliation). Biomedical Engineering Department, Case Western Reserve University, Cleveland, OH, USA.
E-mail addresses: jhimli.mitra@case.edu (J. Mitra), kaikai.shen@csiro.au (K. Shen), soumya.ghose@case.edu (S. Ghose), pierrick.bourgeat@csiro.au (P. Bourgeat), jurgen.fripp@csiro.au (J. Fripp), olivier.salvado@csiro.au (O. Salvado), kerstin.pannek@gmail.com (K. Pannek), jamie.taylor@health.sa.gov.au (D.J. Taylor), jane.mathias@adelaide.edu.au (J.L. Mathias), stephen.rose@csiro.au (S. Rose).

http://dx.doi.org/10.1016/j.neuroimage.2016.01.056
1053-8119/

et al., 2012; Goh et al., 2014; Yeh et al., 2012). As DTI probes the subtle changes in the anisotropic nature of the diffusion of water in white matter (WM), it potentially provides a more sensitive and quantifiable measure of DAI within functionally distinct brain regions, thereby overcoming one of the main limitations of conventional MRI (Huisman et al., 2004). Fractional anisotropy (FA), a widely used quantitative measure of anisotropy, reflects the degree of alignment or organization of axonal pathways and has the potential to identify axonal injury associated with TBI (Johnson et al., 2013). For example, using region of interest (ROI) analyses, significant reduction in FA values in patients with mTBI have been reported within the corpus callosum, internal capsule and centrum semiovale (Kumar et al., 2009; Inglese et al., 2005; Miles et al., 2008; Matsushita et al., 2011). A common finding was a reduction in FA within the genu or splenium of the corpus callosum for mTBI patients. Voxel wise analyses employing Tract-Based Spatial Statistics (TBSS) have revealed more wide spread injury extending to multiple white matter (WM) pathways projecting through the corpus callosum (Kinnunen et al., 2010; Wada et al., 2012). In contrast to ROI or voxel wise analyses, diffusion imaging along with probabilistic tractography allows DAI to be investigated within specific WM pathways associated with multiple neural circuits. This approach is appealing as loss in connectivity of neural networks can be readily computed and may potentially guide the planning of personalized treatment and rehabilitation strategies (Wilde et al., 2006; Xu et al., 2007). Using this approach, number of studies have reported loss of integrity of WM pathways within the corpus callosum, fornix, internal capsule and the peduncular projections in TBI patients compared to normal controls (Wang et al., 2008; Sugiyama et al., 2013).

In recent years, there has been a trend toward using connectome-based strategies to assess the impact of DAI on network connectivity. For example, Pandit et al. (2013) used a graph-theoretic approach based on functional connectivities to show deviation of small-world characteristics i.e. reduced overall connectivity, longer average path lengths and reduced network efficiency in TBI patients compared to control participants, especially within networks involving the posterior cingulate cortex. Their findings also supported previous findings of reduced WM integrity along the corpus callosum, corticospinal tracts and superior longitudinal fasciculi. Similarly, (Caeyenberghs et al., 2013) combined complementary information from the graph-theoretic analysis of the structural and functional hubs to discriminate between the TBI and the healthy groups, with a specific focus on the switching-motor network. Furthermore, graph-theoretic approach using DTI networks was adopted by Irimia et al. (2012a, 2012b) to introduce a patient-tailored approach to the graphical representation of WM change over time. Van Horn et al. (2012) also employed DTI connectomics to study the white matter damage in the simulated case of severe TBI of Phineas Gage, who was an American railroad construction foreman in the 19^{th} century. The study revealed that the impact on measures of network connectivity between the area of direct injury and other areas were profound and widespread, which probably contributed to acute and long-term behavioral changes.

Machine learning approaches are being increasingly used to identify discriminative features from the neural connections that best separate a diseased group from healthy cohorts. For example, Aribisala et al. (2010) applied a region-wise support vector machine (SVM) analysis to identify DAI using T1, T2 maps and mean diffusivity measures in both gray and white matter regions in mTBI patients compared to control participants. Recently, Lui et al. (2014) used features from conventional MRI, diffusion MRI and fMRI to build a set of features and employed a feature selection algorithm prior to applying several classifiers like support vector machines (SVMs), Bayesian networks and multilayer perceptrons to separate mTBI from controls.

Many of the studies in TBI research were based on the use of specific regions known to be associated with the loss of WM integrity in DAI. Such approaches may not identify WM injury elsewhere in more remote brain regions other than the point of impact, which impair a wide array of cerebral functions (Love and Webb, 1992; Gioia et al., 2010). Our limited knowledge of how tract structure relates to cognitive function in normal brain (Kinnunen et al., 2010), leads to the importance of assessment of white matter structure after traumatic brain injury with a highly comprehensive spatial coverage.

Network-based statistical analysis between the TBI and control groups may reveal structural connections based on a stochastic model with the assumption that the mean FA values are different between the groups. These connections being statistically significant in differentiating the two groups, may not however, represent an optimally discriminative feature set in classifying the TBI and control groups due to the following reasons: 1) the exclusive dependence on a stochastic model is an overspecialization when the analysis is performed on a limited number of datasets (Breiman, 2001b). Such an analysis therefore may fail in generalization when validated on a larger cohort. 2) The validation of these statistical methods is usually by goodness-of-fit measures such as hypothesis testing used in network-based statistical analysis (Zalesky et al., 2010). The number of connections obtained with such methods, therefore, may be sensitive to the choice of the threshold used in *t*-tests (Zalesky et al., 2010) and it is often challenging to reach a consensus on how many of these are actually affected due to TBI.

In machine learning, standard feature selection algorithms may find out features or neural connections that are discriminative in classification, while these may not be statistically significant in terms of difference in mean FA values between the TBI and control groups. In other words, the machine learning algorithms do not make any assumption for a data model, instead, a complex, unknown function is learned from the data to predict the responses (Breiman, 2001b). The robust cross-validation schemes used in machine learning approaches, i.e. building a classification model on a training set and validating on a test set, where the sets are mutually exclusive, also provides more confidence and generalization to the analysis. Unleashing the potential of both statistical and machine learning methods, therefore, in this work, we have adopted a hybrid strategy combining both the statistical analysis of network connections and then machine learning in order to identify the cortical/sub-cortical connections that differentiate between TBI patients and age-matched controls.

In our method, we used probabilistic tractography to build structural networks and estimate diffusion anisotropy in a population of TBI (mostly with mTBI) and matched controls, with DAI being characterized by the reduction in diffusion anisotropy (Arfanakis et al., 2002). Network-based statistics (NBS) (Zalesky et al., 2010), which are based on generalized linear model (GLM) and *t*-test statistics, were then applied to extract networks or connections that were different between a subset of the two groups. Tractography data from MRI is very noisy, hence it is very likely that the noise is propagated into pairwise associations measuring FA values over the tracts, thus resulting in a low contrast-to-noise ratio. NBS is known to work better than other generic statistical tests due to its ability to deal with low contrast-to-noise ratio (Zalesky et al., 2010). NBS also involves extensive multiple comparisons correction and reduces the family-wise error rate in a weak sense, which is computationally more expensive in other statistical tests. As discussed before, statistical network separation using *t*-tests is however, sensitive to thresholds. To avoid a precise choice of the *t*-threshold that may vary with datasets, we selected the network from NBS comprising of a large number of structural connections and a high spatial coverage, using a reasonably high *t*-threshold. This ensured that all connections obtained from the NBS network were statistically significant with reduced FA values in TBI than controls.

Retaining a large number of connections may however, present serious challenges to classification methods (Liu and Motoda, 2007), i.e. the curse of dimensionality (Hastie et al., 2001), when many of these obtained from NBS may not be actually predictive in classifying the TBI and healthy groups. With the presence of a large number of features, a classification or prediction model tends to overfit, resulting in

performance degradation on unknown test data (Tang et al., 2014). Selecting the most relevant features is therefore, usually suboptimal in building a good predictor (Guyon and Elisseeff, 2003), especially if the features are correlated and redundant. Principal component analysis (PCA) (Pearson, 1901), a common feature selection technique was therefore, applied on the connections obtained from NBS, in order to reduce and re-express the correlated feature space with a set of linearly uncorrelated components.

Random forest (RF) (Breiman, 2001a) is known to be robust against overfitting and on noisy data. A RF model was therefore, built using the features obtained from NBS and PCA, which was then used to classify the remaining sets of TBI and normal groups that were not used for feature selection using NBS and PCA. The primary advantage of using RF over any other classifier is its uniqueness in providing the feature importance (Gini importance) within the cross-validation scheme based on the training samples. Unlike other traditional feature selection methods, Gini importance is known to capture the multivariate and non-linear relationships among the structural connections and the disease states (Langs et al., 2011) i.e. TBI or non-TBI in our case. Gini importance has been shown to correlate well with the measures based on feature perturbations (Breiman, 2001a; Archer and Kimes, 2008) and known to be stable across datasets without a need for explicit regularization, thereby, providing an alternative to the computationally more expensive statistical permutation tests. All these factors led to a conscientious combination of NBS, PCA and RF classifier that was particularly suited to our problem of finding a comprehensive set discriminative connections with a good spatial coverage that were affected in TBI. The novelty of our method, hence, is in the preliminary selection of signature connections using NBS and then refining the signature connections according to the feature importance provided by the Gini measure of random forest.

Materials and methods

Participants

Data from 179 TBI participants (142 males, age: 42.8 ± 17 yrs. and 37 females, age: 45.8 ± 17.4 yrs) and 146 age-matched controls (81 males, age: 42.5 ± 16.8 yrs. and 65 females, age: 40.3 ± 17.6 yrs). TBI participants were classified as mild (n = 136), moderate (n = 21) and severe TBI (n = 22) following the the Glasgow Coma Scale (GCS) scores. GCS scores for the patients ranged between 1 and 15, with a mean GCS score of 13.1 ± 3.3, which were either recorded by ambulance officers at the accident scene or obtained from hospital records.

Lesions were visible on T1w/T2w MRI in 48 TBI participants. These lesions were characterized by an experienced radiologist (D.J.Taylor) as follows: 8 patients had occasional WM lesions, 13 had ischemic WM lesions or age-related periventricular WM changes, 1 had visible DAI, 5 had haemosiderin foci, 17 had post-traumatic hemorrhages or micro-hemorrhages, 2 had old contusions, 3 had encephalomalacia, 2 had gliosis, 1 had a non-traumatic hemorrhage, and 1 other had an arachnoid cyst. All other TBI patients (n = 131) had normal T1w or T2w MRI.

Imaging data was obtained, on average, 211 ± 77 days post-injury. Control participants included community controls and orthopedic controls who sustained an injury not involving the face or head. All participants were recruited on a prospective basis as part of a larger study of TBI. The local ethics committee approved the study and informed consent was obtained from each participant. No participant reported having a history indicating any developmental, psychiatric or neurological disorders that might independently affect brain structure or function.

Image acquisition

The MRI data were acquired at the Royal Adelaide Hospital (RAH) using a 3 T Siemens TimTrio (Siemens, Erlangen, Germany) scanner with TQ gradients (45 mT/m, SR 200 T/m/s), using commercial sequences from VB15 Neuro applications and Diffusion Tensor Imaging options.

Diffusion images were acquired with the following parameters: 60 axial slices, FOV 25 × 25 cm, TR/TE 9400/116 ms, 2.5 mm slice thickness and acquisition matrix 100 × 100 with a 2.5 mm isotropic resolution. Sixty-five diffusion-weighted images were acquired at each location consisting of 1 low (b = 0) and 64 high (b = 3000 s/mm ^{2}) diffusion-weighted images, in which the encoding gradients were uniformly distributed in space using the electrostatic approach (Jones et al., 1999). The acquisition time for the diffusion scan was 10:41 min. A field map was acquired using two 2D gradient recalled echo images (TE1/TE2 4.76/7.22 ms) to assist the correction for distortion due to susceptibility inhomogeneities.

Data processing

An extensive preprocessing procedure was followed to detect and correct for image artifacts caused by involuntary head motion, cardiac pulsation and image distortions (Pannek et al., 2012b). In brief, image distortions caused by susceptibility inhomogeneities were reduced using the field map, employing the FUGUE (Jenkinson, 2003) and PRELUDE (Jenkinson, 2004) tools that are available with FSL (Jenkinson et al., 2012), and intensity inhomogeneities were removed using N3 correction (Sled et al., 1998). Subsequently, signal intensity outlier voxels (caused by cardiac pulsation, bulk head motion and other artifacts) were detected and replaced using DROP-R (Morris et al., 2011). DROP-R was modified from the originally proposed method to employ a higher order model of the diffusion signal suitable for the detection and replacement of outliers in high b-value diffusion data (HOMOR, (Pannek et al., 2012a)). Between-volume registration to account for head movement during the scan was performed using FMAM (Bai and Alexander, 2008), with adjustment of the b-matrix (Leemans and Jones, 2009; Rohde et al., 2004). Following these steps, FA was estimated from the corrected diffusion data. Constrained spherical deconvolution (Tournier et al., 2007, 2012) (http://nitrc.org/projects/mrtrix) was employed to estimate the fiber orientation distribution for tractography at maximum harmonic order 8.

The 1 mm isotropic T1-weighted subject volumes were first rigidly registered to the respective FA volumes using ANTs, after which the GM, WM and CSF tissues were segmented using an in-house implementation of the model-based segmentation method of van Leemput et al. (1999). In order to initialize and constrain the segmentation, an atlas and associated priors of GM, WM and CSF was typically registered (Ourselin et al., 2002; Modat et al., 2010) to the target T1-weighted volume. An atlas selection (Aljabar et al., 2009) was performed using the Normalized Mutual Information (NMI) between the target volume and the 56 atlases of the Neurodevelopmental MRI Database (Sanchez et al., 2012). The atlas with the highest computed NMI during registration was selected to initialize the segmentation. The subcortical GM structures were subsequently segmented from the T1-weighted volume by non-rigidly registering (Ourselin et al., 2002; Modat et al., 2010) an AAL atlas with 116 regions. Finally, the GM and WM PVE maps were generated using the method of Acosta et al. (2009) and the GM/WM interface and subcortical GM/WM interface PVE maps were thresholded for the seeding strategy, as required in the ACT tractography framework (Smith et al., 2012).

Method

Our approach consisted of two stages: (a) network connectivity analysis for feature selection; and (b) extraction of discriminative features using classification. A schematic diagram depicting these stages is provided in Fig. 1.

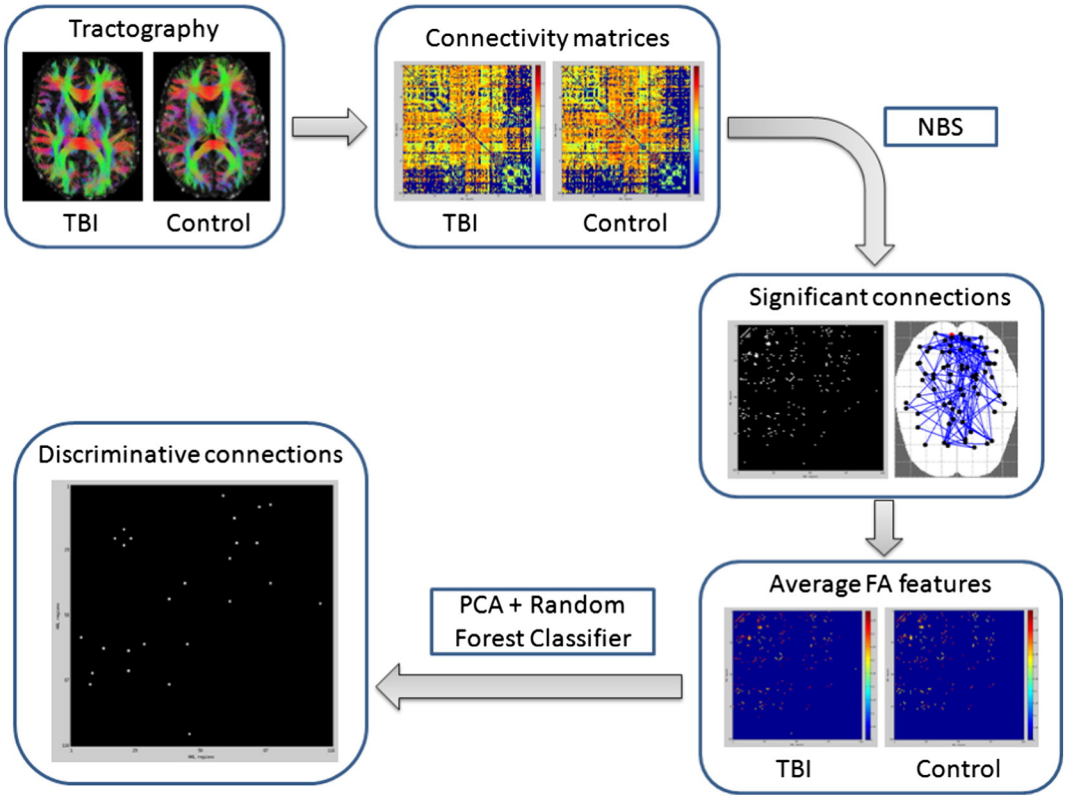

Fig. 1. Schema diagram of our proposed method to find discriminative connections between TBI and healthy populations.

Network connectivity analysis for feature selection

Whole-brain tractography was performed using the probabilistic tractography algorithm MRTrix (Tournier et al., 2012; Smith et al., 2012). This approach uses the Fiber Orientation Distribution technique (FOD) (Tournier et al., 2004) to describe the intra-voxel structures of WM fibers, and anatomically-constrained tractography (ACT) takes advantage of the gray-matter (GM), white-matter (WM) and cerebrospinal fluid (CSF) partial volume estimation (PVE) maps to determine the streamline stopping criterion. In addition, spherical-deconvolution informed filtering (SIFT) (Smith et al., 2013) was used to reduce local bias in streamlines resulting from the seeding strategy, which in this case was the thresholded GM/WM interface obtained from the PVE maps.

In our experiment, ten million probabilistic streamlines were seeded from the GM/WM interface mask using the ACT approach and streamlines were filtered using SIFT until convergence with $\mu = 0.001$. SIFT (Smith et al., 2013, 2015) provides correspondence between the fiber densities estimated from the diffusion model and the reconstructed streamlines densities, therefore the connectivity matrices may be built by directly encoding the number of streamlines connecting the cortical or subcortical regions that is measured by tracing both ends of the streamlines. In terms of measuring the integrity of WM pathways, DAI is often characterized by a decrease in anisotropy and abnormal fractional anisotropy (FA) values in mild to severe TBI (Wada et al., 2012; Caeyenberghs et al., 2010; Kurowski et al., 2009; Aoki et al., 2012; Lipton et al., 2012). Therefore, in our approach, the participant brains were parcellated into 116 regions by non-rigidly registering (Ourselin et al., 2002; Modat et al., 2010) the FA with the T1-weighted Anatomical Atlas Labeling (AAL) atlas and then the tract-averaged FA values, were used to build the 116×116 network connectivity matrix (Pannek et al., 2010; Rose et al., 2012).

Statistical analysis of the brain network was performed using the NBS toolbox for Matlab (https://sites.google.com/site/bctnet/comparison/nbs) (Zalesky et al., 2010) on a subset of TBI ($n = 70$) and control ($n = 40$) groups. The distribution of the mild ($n = 53$), moderate ($n = 8$) or severe ($n = 9$) TBI was similar to that of the entire dataset ($n = 179$). A general linear model was used to identify differences in FA between participant groups for every connection, using age as a confounding variable. NBS assesses the evidence for the null-hypothesis at the cluster level; that is, it controls the family-wise error rate in a weak-sense by isolating an undirected symmetric binary connectivity matrix that significantly differs between participant groups. In our experiment, the output from the NBS analysis provided the list of connections that were likely to be affected when a group-wise network analysis was performed between the TBI patients and the healthy controls. The tract-averaged FA values of these connections were then used as features for the classification between the remaining datasets with TBI ($n = 109$) and controls ($n = 106$) respectively. This strategy ensured mutually exclusive datasets to be used for feature selection and classification.

Extraction of discriminative features using classification

Feature extraction

The aim in using a machine learning approach was to improve the classification of TBI and healthy participants by exploiting the differences in their whole-brain connectivity, and to refine the structural connections that differed between the two populations. In our approach, a feature vector for each participant was first generated using the mean FA values of the structural connections that were identified as significant signatures to separate the two populations from NBS ($t = 2.6, p < 0.002$). Due to matrix symmetry, only the upper triangular matrix of the NBS connectivity matrix was used. Next, a PCA (Pearson,

1901) was applied to the significant neural connections obtained from NBS to project the data on to a new basis in order to maximize the population variability. The principal components, representing 95% variance of the data, that reduced the transformed data to fewer dimensions were retained. Finally, a random forest classification was performed on the transformed feature space to classify the participants and extract a set of refined discriminative features that best separated the TBI from healthy controls. The PCA and the random forest were used within the cross-validation framework, i.e. the model was fitted on the training data and the same model was used to transform the test data.

Classification with random forest (RF)

The transformed data was randomly sampled into training and testing sets for the random forest classifier (http://scikit-learn.org). Random forests (RF) are an ensemble (collection) of decision tree predictors such that the growth of each tree (depth) depends on the values of bootstrapped data sampled independently for all trees in the forest (Breiman, 2001a). In a random forest, each tree node is split using the best variable among a subset of predictors randomly chosen at each node. The optimal threshold and feature are searched in a joint exhaustive search over the threshold and feature spaces. Random sampling of the features (feature-bagging) also leads to increased inter-node and inter-tree variability which improves generalization. The random forest has considerable advantages over other classifiers, e.g. support vector machines (SVMs). It indeed improves the accuracy of probabilistic classification and transparency in feature selection. The averaging of the prediction probabilities of the individual trees leads to improve prediction accuracy. The generalization power increases monotonically with increasing the forest size. The concept of ensemble learning allows RF to learn more complex decision surfaces compared to linear SVMs or those with non-linear kernel functions. Unlike SVM and neural-network, RF also allows to identify the features that are most discriminative by variable permutation testing or Gini impurity. Particularly, the counter-intuitive strategy to form a 'strong' learner, with an ensemble of 'weak learners' (decision trees) in RF, makes it robust against overfitting when compared to many other classifiers including discriminant analysis, support vector machines and neural networks (for more details on RF see Appendix A). A total of 50 trees were used and the tree depth was limited to 15 (experimentally chosen), while only the square-root of the total number of features (default parameter as (Breiman, 2001a)) was used for random-sampling (feature-bagging) at each tree node.

The classifier performance was assessed by K-fold cross validation using the data that were not used for feature selection using NBS. The data i.e. TBI ($n = 109$) and controls ($n = 106$) were randomly partitioned into non-overlapping K groups; in our experiment, K was equal to 10. One group (test) of participants was held out and the remaining K-1 groups were used to train the RF. The test group (21 or 22 subjects) was then used for prediction using the trained model. This scheme of training and testing was repeated until all K-groups were used as test for prediction. The accuracy of the RF classifier was further validated in several K-fold runs, i.e. the experiment was further repeated 100 times to introduce randomness in the cross-validation sets, and ensure robustness and repeatability of the classification. The mean accuracy and standard deviation from 10-fold cross validation iterated over 100 times were used to evaluate the performance of the classifier. In order to validate against overfitting, the number of trees in the forest was varied from 15 to 145 trees, in intervals of 5, and the depth of trees was varied from 5 to 49, in intervals of 2, and the mean accuracies for 100 times validation were recorded.

Discriminative features from RF

The RF algorithm provides feature importance based on the Gini impurity and is defined as the total decrease in node impurity, which is approximated by the proportion of samples reaching a node and averaged over all trees of the ensemble (Breiman et al., 1984). The basic idea is to measure the decrease in accuracy on the out-of-bag (OOB) data when a feature value is randomly permuted. OOB error comes from bootstrapping the training data where at least one-third of the data is left out as test data to calculate the OOB error. If the decrease in OOB error is low, then the feature is not important and vice-versa. This is one unique and statistically robust aspect of RF to get feature importance that is different from SVM. In linear SVM the feature importance is simply the weights of the support vectors on the hyperplane, while, for kernel SVM, the weights are attached to the features in higher dimension, therefore, it is not straightforward to obtain the feature importance. On the other hand, Gini impurity is a quantitative measure to rank the features according to their predictive power. Relevant features based on Gini impurity are considerably more stable and therefore may be used for accurate prediction and as diagnostic features of a disease. The preliminary features used in RF were already obtained through NBS and were of statistical significance. Further identifying the most discriminative features using RF provided a mechanism for refining the features that best separated the TBI and healthy populations.

The features used in RF were in a transformed principal component (PC) space; therefore to map the PC obtained from feature importance of RF back to the network connectivity domain, we used the 'B4' method (Jolliffe, 2002); which is an intuitive and computationally feasible technique and has demonstrated consistent success in the literature (Ziv et al., 2013). In the 'B4' method, a one-to-one correspondence between one feature in the connectivity domain and one PC may be established by selecting the feature with the highest loading or weight in the linear combination of features. In other words, the feature/variable to which the PC was mostly aligned to was identified. In our method, the cumulative feature importance (PCs) obtained from 10-fold runs of RF were ranked in descending order and only the PCs comprising 90 th percentile of the average feature importance measured over 100 repetitions, were considered as discriminative features. Each PC feature was then mapped to a variable in the network connectivity domain using the 'B4' method.

Validation strategy

As a method of comparison and to justify our strategy to identify discriminative neural connections using NBS in conjunction with standard machine learning approach (NBS-PCA-RF), we have compared our proposed method with the following variations: 1) random forest used on raw connectivity matrices (RF-Raw), 2) random forest with dimensionality reduction using PCA on raw connectivity matrices (RF-PCA-Raw), and 3) random forest on features preselected from NBS with a moderately high t-test threshold (NBS-RF, $t = 2.6$). Additionally, to justify that GLM based methods may not guarantee generalization in the presence of noisy measurements and may not provide discriminative features for the best separation of two groups, 4) we analyzed the classification performance on features selected by NBS using a very high t-test threshold (NBS-RF-hard, $t = 3.0$). The same set of RF parameters was used for all the above variations of the proposed method for fair comparison. In order to test the null hypothesis that the methods we compared had significantly different mean accuracies, we used the one-way ANOVA (Analysis of Variance) test.

We have also compared the performance of the RF classifier over commonly used classifiers like SVM. SVM (Vapnik and Lerner, 1963; Vapnik and Chervonekis, 1964; Boser et al., 1992) is the most widely used classifier in machine learning domain due to its simple and intuitive formulation. The classifier tries to find a hyperplane the separates two classes while maximizing the margin of separation between the two classes. The soft margin method (Cortes and Vapnik, 1995) used here optimally fits a hyperplane that splits the data samples as cleanly as possible, while still maximizing the distance to the nearest cleanly split samples. We have used a linear SVM classifier (L-SVM) and two non-linear classifiers with radial-basis (K-SVM-RAD) and polynomial kernel functions (K-SVM-POLY2 and K-SVM-POLY3) respectively. The linear SVM tries to fit a maximum-margin hyperplane on the original

feature-space, while the kernel SVM fits the hyperplane in the high-dimensional feature space transformed by the kernels. The radial-basis function in K-SVM-RAD used is a Gaussian function while the polynomial kernels used are of degree 2 (K-SVM-POLY2) and degree 3 (K-SVM-POLY3) respectively. The default penalty parameter $C=1.0$ was used for both linear and kernel SVMs, while the kernel coefficient $\gamma=1/$ *number_of_features* was used for the kernel SVMs. The same set of features as obtained from NBS were used, and a PCA was also performed within the 10-fold cross-validation framework, repeated 100 times for a fair comparison with the RF classifier. All SVM classification algorithms were run using the Python scikit machine learning library (scikit-learn.org).

It is known that NBS provides a cluster of network connections that is significantly different between two groups from a set of suprathreshold edges. This means that the each of these connections that were obtained from NBS with TBI (n = 70) and controls (n = 40), satisfied the null-hypothesis that TBI subjects have reduced FA than controls. In order to further verify the statistical significance of the discriminative connections obtained from RF classification, we evaluated the null-hypothesis that the mean tract-averaged FA values are higher in the controls (n = 106) than the TBI (n = 109).

The classification performance of our proposed method and other variations were evaluated using the standard measures sensitivity (TPR), false positive rate (FPR), positive predictive value (PPV), negative predictive value (NPV), and accuracy (ACC). More details on the evaluation measures are shown in Appendix B.

Results

Network connectivity analysis

A group-wise *t*-test comparison between the TBI (n = 70) patients and the age-matched controls (n = 40), performed using NBS, provided a list of statistically significant neural connections with $p<0.002$ at $t=2.60$. Fig. 2 shows the significant connections as network graphs obtained from NBS. A total of 115 connections were identified as being significantly different between the two groups, which were eventually reduced and refined by PCA and RF, respectively. A higher threshold used for NBS ($t=3.0$) revealed 30 significant connections (Fig. 3). A list of these connections is provided in Table 1.

Classification and discriminative features

Fig. 4 shows the accuracies over the random forest parameters. It was observed that the mean accuracy was restricted to around 68%

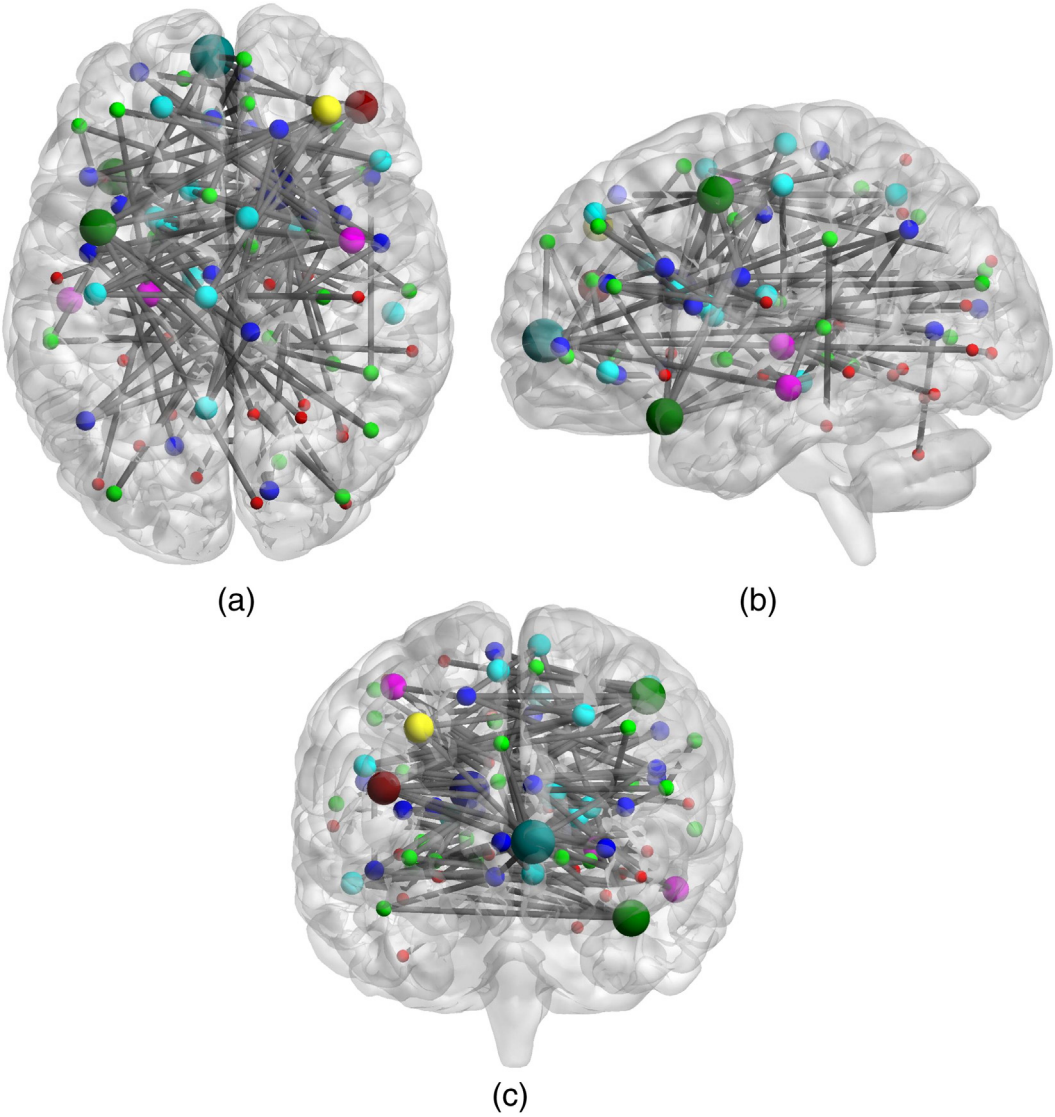

Fig. 2. Significant network connections with $p<0.002$ obtained from NBS with *t*-test threshold 2.6. Figures (a), (b) and (c) show NBS connectivity graph for the significant network connections in axial, sagittal and coronal views respectively. Node sizes represent the degree of each node, i.e. larger nodes represent higher impact of DAI on cortical region.

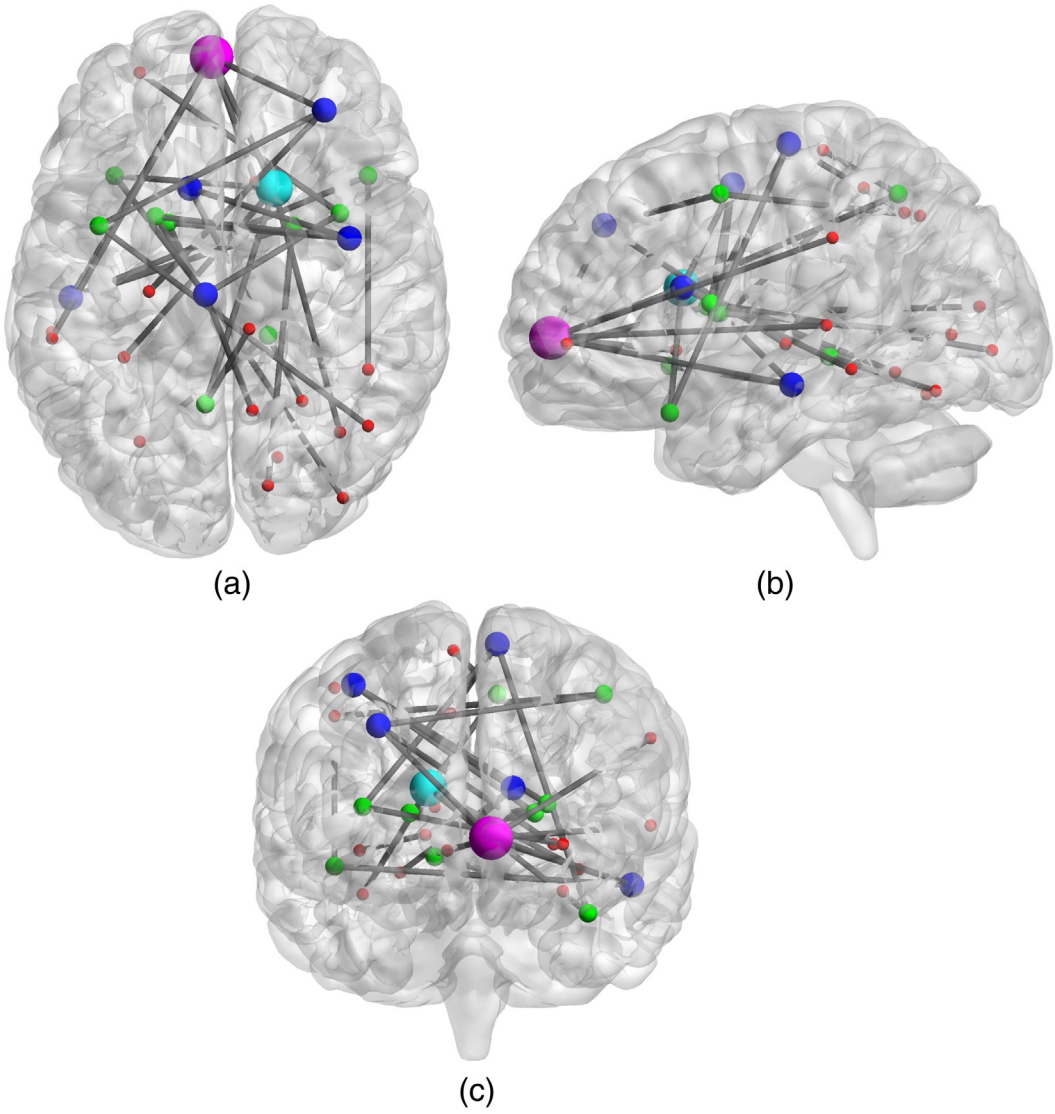

Fig. 3. Significant and perhaps non-discriminative network connections with $p<0.001$ obtained from NBS with t-test threshold 3.0. Figures (a), (b) and (c) show NBS connectivity graph for the significant network connections in axial and sagittal views respectively. Node sizes represent the degree of each node, i.e. larger nodes represent higher impact of DAI on cortical region.

after 50 trees and varying the depth did not actually affect the mean accuracy. The highest accuracy was observed around the depth of 15, therefore to further reduce the chance of overfitting we fixed the tree depth to 15 as mentioned before.

Table 2 shows the list of discriminative 25 neural connections that best separated the TBI (n = 109) and healthy control (n = 106) groups. These connections were based on the average Gini impurity measures across 10-fold validation, repeated 100 times. The table also shows the significance of the t-tests performed to test the null-hypothesis that the mean FA values for the obtained discriminative connections are higher in controls than the TBI group. It was observed that most of the connections obtained from RF Gini impurity were significant with $p<0.05$, while only a few with $p<0.1$. For visualization purposes, the cortical/subcortical regions associated with the connections that were discriminative between the TBI subjects with DAI and the control groups in Table 2 are shown in Fig. 5.

Table 3 shows the evaluation measures for the proposed and other variations using RF. It was observed that our proposed approach (NBS-PCA-RF) provided the highest classification accuracy and high sensitivity in correctly classifying TBI patients, compared to all other variations. It was also observed that feature selection with NBS at a high threshold of $t = 3.0$ provided few statistically significant neural connections, but these connections did not show enough discriminative power to separate the two groups (refer to the NBS-RF-hard row in Table 3). Please note that the results for the first 2 rows were obtained using TBI (n = 179) and controls (n = 146) as NBS was not involved in these method variations, while the remaining rows show the validation done on the remaining TBI (n = 109) and control (n = 106) datasets after NBS.

The one-way ANOVA test supported the null hypothesis that the alternative methods have significantly different means ($p<0.0001$). Fig. 6 shows the box plot of the mean accuracies of the methods that were compared, together with 95% confidence intervals. Additionally, Dunn's post-hoc test was performed with Bonferroni correction to compare between the mean accuracies of the proposed and other methods. This post-hoc test revealed that the proposed method (NBS-PCA-RF) had significantly better mean accuracy than any of the other variations ($p<0.01$).

Table 4 shows the classification accuracies using NBS on TBI (n = 70) and controls (n = 40), followed by PCA and linear SVM or kernel SVMs with radial and polynomial basis functions. All results shown in this table were validated on the remaining datasets after NBS i.e. TBI (n = 109) and controls (n = 106).

It was observed that linear SVM provided similar classification accuracy as NBS-PCA-RF with slightly less true positives i.e. the patients with

Table 1
Neural connections obtained from NBS that are significantly different between the TBI (n = 70) and healthy populations (n = 40) using a high *t*-threshold of 3.0 and $p<0.001$. The regions are labeled according to the AAL atlas with 116 regions. Acronyms for the connections are given in Appendix C.

Inter-hemispheric connections (Left ↔ Right)	
PreC_G	Mid_Fron_G
PreC_G	Ang_G
Caud_Nuc	PreC_G
Lent_Nuc_Put	PreC_G
Lent_Nuc_Pall	PreC_G
Sup_Fron_G_Med_Orb	Mid_Fron_G
Hippocampus	Mid_Fron_G
Mid_Fron_G_Orb_Part	Insula
Sup_Fron_G_Med_Orb	Olfac_Cortex
Sup_Fron_G_Med_Orb	Caud_Nuc
ParaC_Lobule	Insula
Lenti_Nuc_Pall	Lingual_G
Lent_Nuc_Put	Inf_Occi_G
Fusiform_G	Caud_Nuc
Precuneus	ParaC_Lobule
Precuneus	Caud_Nuc
ParaC_Lobule	Precuneus
Caud_Nuc	Cerebelum_3
Caud_Nuc	Cerebelum_6
Temp_Pole_Mid_Temp_G	Caud_Nuc
Inf_Temp_G	Lent_Nuc_Pall
Inf_Temp_G	Temp_Pole_Sup_Temp_G
Cerebelum_Crus1	Cerebelum_3
Intra-hemispheric connections (left)	
Sup_Fron_G_Med_Orb	SupraMarg_G
Sup_Fron_G_Med_Orb	Mid_Temp_G
Sup_Fron_G_Med_Orb	Inf_Temp_G
ParaC_Lobule	Temp_Pole_Mid_Temp_G
Intra-hemispheric connections (right)	
Calc_Fiss_&_Surr_Cortex	Lent_Nuc_Pall
Inf_Parietal_G	Temp_Pole_Sup_Temp_G
Caud_Nuc	Cerebelum_Crus1

Table 2
Neural connections obtained from our proposed method NBS-PCA-RF that were most discriminative to best separate the TBI (n = 109) and healthy (n = 106) populations. The regions are labeled according to the AAL atlas with 116 regions. The connections were statistically significant as predetermined from NBS ($p<0.002$, $t=2.6$, TBI (n = 70), controls (n = 40)), random forest further provided the respective cumulative feature importance (%) in discriminative classification using 10-fold cross validation. The last column shows the *p*-value significance of the null hypothesis that mean FA of the controls (n = 106) are higher than TBI (n = 109) with DAI. These connections were obtained after averaging the results from 10-fold cross-validation, repeated 100 times. Acronyms for the connections are given in Appendix C.

Inter-hemispheric connections (left ↔ right)		Feat.Imp.	FA (p)
Lent_Nuc_Pall	PreC_G	98.324	0.0032
PostC_G	Hippocampus	28.143	0.0491
Ang_G	Inf_Temp_G	24.559	0.0013
Ang_G	Lent_Nuc_Pall	24.218	0.0003
Hippocampus	Mid_Fron_G	24.171	0.0076
Caud_Nuc	Cerebelum_3	23.373	0.0019
Precuneus	Caud_Nuc	22.626	0.0006
PreC_G	Cuneus	21.504	0.0138
PreC_G	Ang_G	20.045	0.0001
Sup_Fron_G_Med_Orb	Olfactory_cortex	19.439	0.0093
Hippocampus	PostC_G	18.582	0.0062
PreC_G	Temp_Pole_Sup_Temp_G	17.69	0.0999
Inf_Fron_G_Oper_Part	Caud_Nuc	17.441	0.0713
Inf_Fron_G_Tri_Part	Caud_Nuc	17.318	0.0071
Calc_Fiss_&_Surr_Cortex	Insula	16.599	0.0132
Inf_Temp_G	Inf_Parietal_G	16.365	0.0352
Mid_Temp_G	Mid_Temp_G	16.319	0.0355
ParaC_Lobule	Mid_Fron_G	16.26	0.0083
Lent_Nuc_Put	Lingual_G	15.927	0.0546
Hippocampus	Mid_Occi_G	15.485	0.0268
Inf_Fron_G_Oper_Part	Inf_Fron_G_Tri_Part	15.304	0.0112
Lent_Nuc_Put	Inf_Occi_G	15.033	0.0016
Intra-hemispheric connections (left)			
Sup_Fron_G_Med_Orb	Inferior_Occi_G	16.592	0.0022
Ant_Cing_&_ParaCing_G	Temp_Pole_Sup_Temp_G	15.643	0.0015
Intra-hemispheric connections (right)			
Inf_Parietal_G	Temp_Pole_Sup_Temp_G	15.556	0.0048

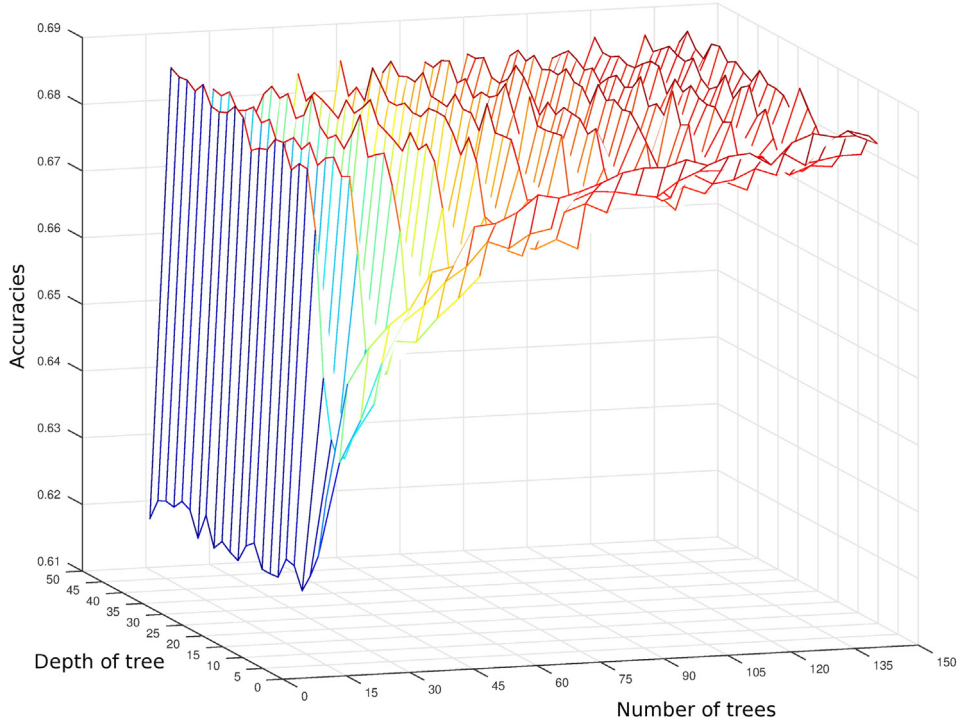

Fig. 4. Mean accuracies for the classification over 10-fold validation run 100 times with varying random forest parameters.

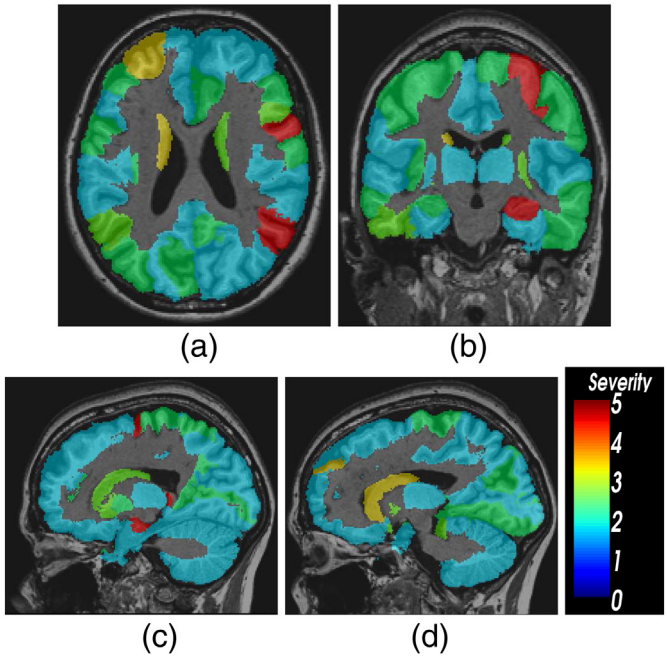

Fig. 5. Cortical and subcortical regions associated with DAI as obtained from RF Gini impurity. These regions were obtained from the average set of discriminative connections as shown in Table 2. Figures (a) and (b) are the axial and coronal views of the affected areas, while (c) and (d) show the affected cortical and subcortical areas in sagittal views for left and right hemispheres respectively. 'Blue' to 'red' denotes increased level of severity. Severity was measured as the number of discriminative connections separating TBI from controls, which end at or emanate from the cortical/subcortical regions.

TBI were not correctly identified. The RBF kernel of SVM although, provided high accuracy with less false positives but the number of true positives were also reduced, i.e. less TBI subjects were identified correctly. The polynomial basis kernels of SVM with both degree 2 and 3 however, could not discern between TBI and non-TBI properly that is evident from the increased false positive rates.

Discussions

In this study we proposed a novel method to classify TBI and healthy control participants, and identified the statistically significant and discriminative structural connections between the two populations using a machine learning approach. NBS was used to identify statistically significant brain network differences between TBI and normal controls. The results from the NBS analysis revealed injury to a number of intra- and inter-hemispheric WM pathways known to be associated with DAI (Wada et al., 2012). These include WM pathways associated with the corpus callosum, the fornix and superior frontal gyri connections. In terms of feature selection for the machine learning algorithm, the choice of the t-threshold to cluster the nodes in NBS was found to be of critical importance. Too low a threshold can produce numerous links between the nodes, where as a higher threshold enabled extraction of a more conservative set of node connections. However, it is important to highlight that these significant connections may not adequately discriminate between the TBI and normal control groups. To better understand the impact of threshold level, we experimented with NBS t-threshold values in the range of 2.0 to 3.1 and used the mean FA of the significant connections for PCA and random forest classification. The most discriminative classification was obtained at $t = 2.6$. We also performed PCA for feature decorrelation instead of reduction on the 30 connections obtained from NBS ($t = 3.0$), but the classification accuracy obtained finally with RF was similar to NBS-RF-hard (i.e. without PCA). Threshold levels in NBS may produce local networks that are of statistical significance, however this may remove some important connections that serve to discriminate between TBI and healthy control groups.

Statistical and machine learning approaches like t-test statistics, PCA, support vector machines and linear discriminant analysis have been effective and have been widely used in neuroimaging studies (Costafreda et al., 2009; Dosenbach et al., 2010; Robinson et al., 2010; Wang et al., 2012; Liu et al., 2012; Fang et al., 2012). Most of these methods aimed at linear separability of the data, to identify the maximum brain differences depending on the hyperplane separating the groups. The analysis made by Aribisala et al. (2010) revealed differences in overall white matter with high sensitivity between mTBI and controls using features like quantitative T1, T2 maps and the mean diffusivity maps. The recent investigation by Lui et al. (2014) using machine learning, showed high accuracy of 86% in separating TBI from controls involving a small cohort and a different set of features derived from multimodal MRI. The relevant features obtained using maximal-relevance minimal redundancy method were features involving thalamic and cortical volumes and magnetic field correlation. None of these previous investigations using diffusion MRI and machine learning methods did aim to identify the structural connections that were affected due to diffuse axonal injury which, is the primary aim of our work i.e. using the Gini impurity to determine the discriminative predictive power of the features during the boot-strapped training procedure of RF.

The use of NBS in our approach guaranteed maximum differences in brain networks with statistical significance, while feature-bagging and boot-strapping methods of random forest classifier ensured a high classification rate and generalization. Therefore, in this study, random forest has been used as a method of refinement of the significant neural connections to a list of discriminative connections. A primary advantage of random forest is its aim to reduce the training OOB error by the feature-bagging, therefore it is likely that the same sets of important features were extracted in each fold. This also guaranteed the repeatability of the classifier. Additionally, the use of PCA for dimensionality reduction has increased the classification accuracy as evident from Table 3.

Experiments were performed to find the discriminative connections directly from the raw FA features of the connectivity matrices as in RF-Raw and RF-PCA-Raw. We observed in Table 3, however, that the accuracies of both RF-Raw and RF-PCA-Raw were lower than NBS-PCA-RF. This means the optimality of the RF training was compromised in the presence of noisy feature measurements, while the classification accuracies improved when features from NBS were used (observed in NBS-RF-hard, NBS-RF and NBS-PCA-RF). Although NBS is sensitive to

Table 3
Quantitative performance measures of our proposed method when compared to other variations. These are the average results from 10-fold cross validation repeated 100 times. All measures are shown as percentages (%). The evaluation in the first two rows include TBI (n = 179) and controls (n = 146), while those in the remaining rows were evaluated on TBI (n = 109) and controls (n = 106) respectively as NBS was involved in these methods.

Method	TPR	FPR	PPV	NPV	ACC
RF-Raw	73.97 ± 2.61	52.32 ± 3.58	63.72 ± 1.90	59.62 ± 3.24	62.24 ± 2.32
RF-PCA-Raw	75.34 ± 3.25	64.09 ± 3.81	59.35 ± 1.68	54.03 ± 4.01	57.75 ± 2.34
NBS-RF-hard	75.56 ± 2.29	44.39 ± 2.43	67.61 ± 1.35	65.03 ± 2.34	66.59 ± 1.64
NBS-RF	72.43 ± 2.16	42.27 ± 2.92	67.77 ± 1.69	63.08 ± 2.24	65.82 ± 1.82
NBS-PCA-RF	80.0 ± 2.36	46.07 ± 2.96	68.0 ± 1.51	68.54 ± 2.77	68.16 ± 1.81

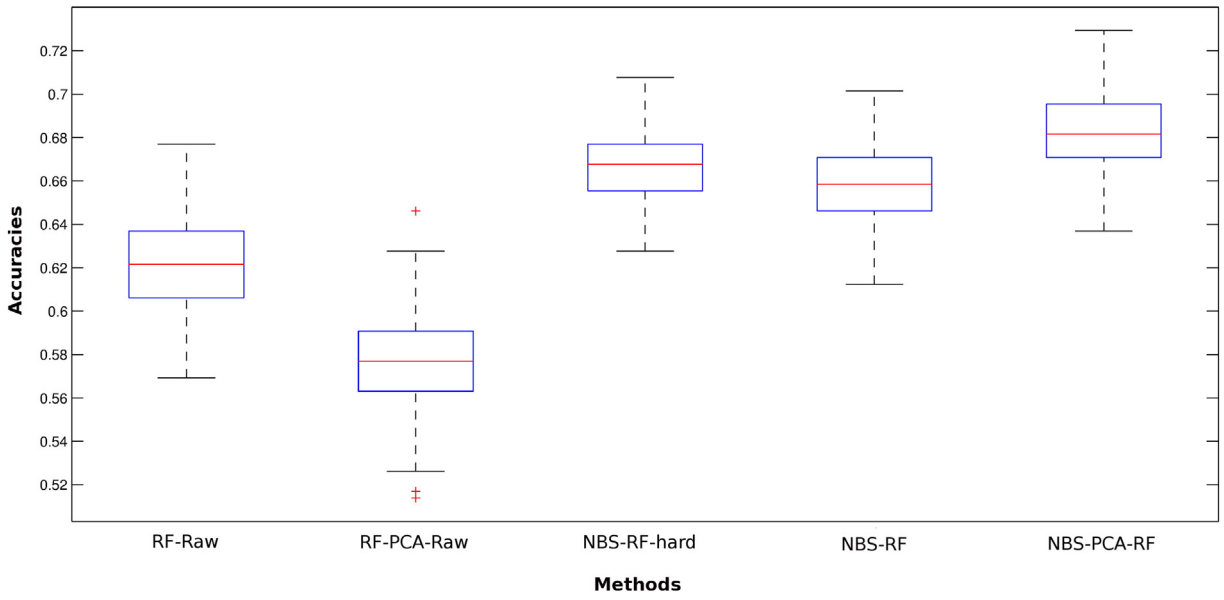

Fig. 6. Box-plot of the mean accuracies for the compared methods with 95% confidence interval obtained from 10-fold cross-validation, repeated 100 times.

threshold, they provide a set of significant connections that well characterize the differences between the TBI and control groups with a particular confidence level. Thereafter, random forest classification with these features identified a list of connections with their respective importance levels in differentiating between the groups. The comparison with L-SVM and NBS-PCA-RF showed similar performance in accuracy. The true positive rate i.e. the predictive power to identify TBI correctly however, was compromised in L-SVM. Besides, L-SVM provides variable importance as the weights of the features (support vectors) on the hyperplane, that does not directly give a notion of the predictive power of a feature variable, unless SVM is explicitly used for feature selection as in SVM-RFE (SVM Recursive Feature Elimination) (Guyon et al., 2002). Gini impurity in RF on the other hand, provides a statistically robust measure of the predictive power of each variable and has been known to perform better than SVM-RFE in some cases (Langs et al., 2011). Kernel SVMs (K-SVM-RAD, K-SVM-POLY2 and K-SVM-POLY3) did not show high accuracies compared to NBS-PCA-RF. The possible reason for this may be the inherently complex decision surface between the TBI and the healthy controls, and simply transforming the data into higher dimension with the kernels could not discern a hyperplane with maximum-margin separation between the groups. Therefore, considering all these aspects, for our experiments, RF has been a better choice than SVM.

To the best of our knowledge, this is the first study using a combination of statistical analysis and machine learning to find discriminative and statistically significant structural connections that are affected due to TBI. The discriminative structural connections identified using our method corroborated the findings reported by Adams et al. (1982, 1986) and Wada et al. (2012), Pandit et al. (2013), Kumar et al. (2009), Inglese et al. (2005), Miles et al. (2008), Matsushita et al. (2011), where DAI was mostly found within the corpus callosum, fornix, connections in superior frontal gyri, cerebellum and dorsal quadrants. The network connections identified using our method show inter-hemispheric connections that are disrupted in DAI. This suggests disruption in the callosal bundles or the fornix and hence, resulting in reduced FA in these areas, similar to what was reported in most of the previous studies (Pandit et al., 2013; Irimia et al., 2012a; Van Horn et al., 2012). We also observed disruption in fiber connections to, or emanating from the cingulate cortices that corroborate the research findings in Kinnunen et al. (2010), suggesting cognitive impairment in DAI to be associated with reduced FA in the anterior cingulate cortex. The fiber connections projecting from the striatum (caudate nucleus and pallidum) to the cortical gyri also suggest involvement of the anterior limb with reduced FA in discriminating mTBI from controls (Kasahara et al., 2012). The discriminative connections from the angular gyri in the parietal lobe to the temporal and frontal lobes suggest involvement of the superior longitudinal fasciculus (Pandit et al., 2013) that is specifically known to be associated reduced cognitive functions in mTBI exhibiting reduction in FA (Kraus et al., 2007). The insula is known to be associated with emotion, perception and other cognitive functions, many of which manifest as clinical phenotypes associated with TBI. Therefore, our findings of discriminative connections running to or from the insula strongly associate the loss in white-matter integrity in this region due to DAI. Further, the inter-hemispheric connections from the hippocampus to the frontal gyri suggest the involvement of fornices that are also known to be involved in the impairment of cognitive functions due to DAI (Kinnunen et al., 2010).

Although, the impact of TBI is profound and widespread in remote brain regions other than the direct site of injury, most studies involving multifocal DAI revealed a commonality in the affected areas in the genu, splenium of the corpus callsoum, parasagittal white matter and the brainstem (Wang et al., 2008; Wada et al., 2012; Pandit et al., 2013). Following the same idea, our goal in this work has been to uncover such frequently affected areas with a larger spatial coverage and to

Table 4
Quantitative performance measures of our proposed method with RF compared to linear and kernel SVMs. The results are averaged over 10-fold cross validation repeated 100 times. The evaluations were done on TBI (n = 109) and controls (n = 106) as all these methods involved a prior feature selection using NBS. All measures are shown as percentages (%).

Method	TPR	FPR	PPV	NPV	ACC
L-SVM	77.96 ± 0.72	46.87 ± 0.55	67.65 ± 0.30	68.38 ± 0.78	67.90 ± 0.43
K-SVM-RAD	73.42 ± 0.69	33.43 ± 0.65	72.92 ± 0.34	67.14 ± 0.52	70.34 ± 0.36
K-SVM-POLY2	92.32 ± 2.59	86.72 ± 3.14	56.63 ± 0.67	58.91 ± 0.56	56.81 ± 1.15
K-SVM-POLY3	94.91 ± 1.71	80.92 ± 3.84	59.0 ± 0.90	75.66 ± 3.51	60.84 ± 1.26
NBS-PCA-RF	80.0 ± 2.36	46.07 ± 2.96	68.0 ± 1.51	68.54 ± 2.77	68.16 ± 1.81

measure the degree of impact in such regions due to DAI. Identifying precise neural connections with loss in WM integrity due to DAI using our method, would essentially facilitate a better understanding of the long-term cognitive and behavioral impacts due to the disease, and hence, may aid in developing successful rehabilitation strategies even before the symptoms of DAI appear. We do however, understand that patient-specific personalized therapies may be necessary for faster recovery due to heterogeneity of the location of TBI that requires evaluation of affected brain regions on individual patients (Feng et al., 2010; Rosenbaum and Lipton, 2012; Bouix et al., 2013). This is currently a limitation of our research and we will consider developing a methodology to highlight patient-specific impacted areas due to TBI as a part of our future works.

In conclusion, this study has provided a statistically robust method for the analysis and classification of the whole brain network of microscopic neural connections. The approach allows accurate classification between large groups of participants. Features extracted using network-based group-wise patient/control analysis have the potential for highlighting important tracts that differentiate between groups, while classifiers built on such features may have the potential for robust classification and disease diagnosis, which may further improve our understanding of disease progression.

Acknowledgments

This research was funded by a National Health and Medical Research Project Grant (ID 519220). The authors wish to thank Ms. V. Dennington and Dr. Y. Harman-Smith for their efforts in subject recruitment.

Appendix A. Random forest (RF)

A.1. RF training

The training data consists of a feature set of tract-averaged FA values of the significant connections $v_k \in \mathbb{V}$ with associated label $Y(v_k)$. The forest is composed of T trees with t indexing each tree. During training, the full feature set $\mathbb{V}$ is pushed through each of the trees. Each node p receives a random partition of feature set $\mathbb{V}_p$. An optimal test threshold λ_p^*, found by exhaustive search over the randomly sampled feature space and uniformly discretized threshold space ($\lambda_p \in \tau_p$) is used to split the feature set $\mathbb{V}_p$ into the left and right child nodes respectively. The test threshold is optimized by maximizing the information gain ζ_p defined for discrete distributions as follows:

$$\lambda_p^* = \arg\max_{\lambda_p \in \tau_p} \zeta_p, \tag{A.1}$$

$$\zeta_p = H(\mathbb{V}_p) - \sum_{i \in \{L,R\}} \frac{\left|\mathbb{V}_p^i\right|}{\left|\mathbb{V}_p\right|} H\left(\mathbb{V}_p^i\right) \tag{A.2}$$

with i indexing the two child nodes. The entropy for a generic set of $\mathbb{V}$ of training points is defined as:

$$H(\mathbb{V}) = -\sum_{c \in \mathbb{C}} p(c) \log p(c) \tag{A.3}$$

where $p(c)$ is calculated as normalized empirical histograms of the labels $c \in \mathbb{C}$ corresponding to the training points in $\mathbb{V}$.

Trees are grown to a maximum depth D which can be full-grown trees or until the information gain is below a minimal value. At the end of the training process, each leaf node l_t contains a class predictor as.

$$P_{l_t}(Y(v) = c) = \frac{\left|\mathbb{V}_{l_t}^c\right|}{\left|\mathbb{V}_{l_t}\right|} \tag{A.4}$$

which is the fraction of points of each class c in the $\mathbb{V}_{l_t}$.

A.2. Classification with RF

For a new test dataset each sample feature v_k is propagated through all trees T by successive application of the learned split functions. After reaching a leaf node l_t in all trees $t \in [1 \ldots T]$, the posteriors $P_{l_t}(Y(v) = c)$ of belonging to a class $c \in \mathbb{C}$ are gathered in order to compute the final posterior probability defined as follows:

$$P(Y(v) = c) = \frac{1}{T} \sum_{t=1}^{T} P_{l_t}(Y(v) = c) \tag{A.5}$$

which is the mean over all the trees in the forest. In this work, the predicted class is the weighted majority vote given by the posterior probability P_c.

Appendix B. Evaluation measures

The notations used for evaluation are TP = true positives, TN = true negatives, FP = false positives and FN = false negatives. The true positive rate (TPR), also called as the recall rate or sensitivity, measures the proportion of actual positives (TBI patients) which are correctly classified as such and is measured by.

$$TPR = \frac{TP}{TP + FN}. \tag{B.1}$$

The false positive rate (FPR), also called as the precision or 1-sensitivity, measures the proportion of false positives, in this case the number of healthy controls incorrectly identified as TBI patients. FPR is computed as.

$$\mathrm{FPR} = \frac{FP}{FP + TN} \tag{B.2}$$

The positive predictive value or the precision rate (PPV) denotes the proportion of true positives i.e. the patient classified as TBI patient has actually suffered TBI and is given by.

$$\mathrm{PPV} = \frac{TP}{TP + FP}. \tag{B.3}$$

The negative predictive value (NPV) denotes the proportion of true negatives i.e. a subject classified as healthy is actually a normal control and is measured as.

$$\mathrm{NPV} = \frac{TN}{TN + FN}. \tag{B.4}$$

The accuracy (ACC) determines the overall accuracy of a method in classifying both TBI (TP) and healthy controls (TN) successfully and is given by.

$$\mathrm{ACC} = \frac{TP + TN}{TP + FP + TN + FN}. \tag{B.5}$$

Appendix C. Network connection acronyms

Ang_G — Angular Gyrus.
Ant_Cing_&_ParaCing_G — Anterior Cingulate and Paracingulate Gyri.
Calc_Fiss_&_Surr_Cortex — Calcarine Fissure and Surrounding Cortex.
Caud_Nuc — Caudate Nucleus.
Fusiform_G — Fusiform Gyrus.
Inf_Fron_G_Oper_Part — Inferior Frontal Gyrus Operculum Part.
Inf_Fron_G_Tri_Part — Inferior Frontal Gyrus Triangular Part.

Inf_Occi_G — Inferior Occipital Gyrus.
Inf_Parietal_G — Inferior Parietal Gyrus.
Inf_Temp_G — Inferior Temporal Gyrus.
Lingual_G — Lingual Gyrus.
Mid_Fron_G — Middle Frontal Gyrus.
Mid_Fron_G_Orb_Part — Middle Frontal Gyrus Orbital Part.
Mid_Temp_G — Middle Temporal Gyrus.
Lent_Nuc_Pall — Lenticular Nucleus Pallidum.
Lent_Nuc_Put — Lenticular Nucleus Putamen.
Olfac_Cortex — Olfactory Cortex.
ParaC_Lobule — Paracentral Lobule.
PreC_G — Precentral Gyrus.
PostC_G — Postcentral Gyrus.
Sup_Fron_G_Med_Orb — Superior Frontal Gyrus Medial Orbital.
SupraMarg_G — Supramarginal Gyrus.
Temp_Pole_Mid_Temp_G — Temporal Pole Middle Temporal Gyrus.
Temp_Pole_Sup_Temp_G — Temporal Pole Superior Temporal Gyrus.

References

Acosta, O., Bourgeat, P., Zuluaga, M., Fripp, J., Salvado, O., Ourselin, S., 2009. Automated voxel-based 3D cortical thickness measurement in a combined Lagrangian–Eulerian PDE approach using partial volume maps. Med. Image Anal. 13, 730–743.

Adams, J.H., Graham, D.I., Murray, L.S., et al., 1982. Diffuse axonal injury due to nonmissile head injury in humans: an analysis of 45 cases. Ann. Neurol. 12, 557–563.

Adams, J.H., Doyle, D., Graham, D.I., et al., 1986. Deep intracerebral (basal ganglia) haematomas in fatal non-missile head injury in man. J. Neurol. Neurosurg. Psychiatry 49, 1039–1043.

Aljabar, P., Heckemann, R., Hammers, A., Hajnal, J., Rueckert, D., 2009. Multi-atlas based segmentation of brain images: atlas selection and its effect on accuracy. NeuroImage 46, 726–738.

Aoki, Y., Inokuchi, R., Gunshin, M., Yahagi, N., Suwa, H., 2012. Diffusion tensor imaging studies of mild traumatic brain injury: a meta-analysis. J. Neurol. Neurosurg. Psychiatry 83, 870–876.

Archer, K., Kimes, R., 2008. Empirical characterization of random forest variable importance measures. Comput. Stat. Data Anal. 52, 2249–2260.

Arfanakis, K., Haughton, V.M., Carew, J.D., Rogers, B.P., Dempsey, R.J., Meyerand, M.E., 2002. Diffusion tensor mr imaging in diffuse axonal injury. Am. J. Neuroradiol. 23, 794–802.

Aribisala, B.S., Cowie, C.J.A., He, J., Wood, J., Mendelow, A.D., Mitchel, P., Blamire, A., 2010. Classification of traumatic brain injury patients using multi-parametric automatic analysis of quantitative MRI scans. Intl. workshop on medical Imaging and Augmented Reality, pp. 51–59.

Bai, Y., Alexander, D., 2008. Model-based registration to correct for motion between acquisitions in diffusion MR imaging. IEEE Intl. Symposium on Biomedical imaging: From nano to macro, pp. 947–950.

Benson, R., 2012. Detection of hemorrahagic and axonal pathology in mild traumatic brain injury using advanced MRI: implications for neurorehabilitation. NeuroRehabilitation 31, 261–279.

Bigler, E., Maxwell, W., 2012. Neuropathology of mild traumatic brain injury: relationship to neuroimaging findings. Brain Imaging Behav. 6, 108–136.

Boser, B., Guyon, I., Vapnik, V., 1992. A Training Algorithm For Optimal Margin Classifiers, In: Proc. Of the 5th annual Workshop On Computational Learning Theory (COLT'92). pp. 144–152.

Bouix, S., Pasternak, O., Rathi, Y., Pelavin, P.E., Zafonte, R., Shenton, M.E., 2013. Increased gray matter diffusion anisotropy in patients with persistent post-concussive symptoms following mild traumatic brain injury. PLoS One 8, e66205.

Breiman, L., 2001a. Random forests. Mach. Learn. 45.

Breiman, L., 2001b. Statistical modeling: the two cultures. Stat. Sci. 16, 199–231.

Breiman, L., Friedman, J., Olshen, R., Stone, C., 1984. Classification and Regression Trees. Wadsworth and Brooks, Monterey, CA.

Caeyenberghs, K., Leemans, A., Geurts, M., Taymans, T., Linden, C.V., Smits-Engelsman, B.C.M., Sunaert, S., Swinnen, S.P., 2010. Brain–behavior relationships in young traumatic brain injury patients: fractional anisotropy measures are highly correlated with dynamic visuomotor tracking performance. Neuropsychologia 48, 1472–1482.

Caeyenberghs, K., Leemans, A., Leunissen, I., Michiels, K., Swinnen, S., 2013. Topological correlations of structural and functional networks in patients with traumatic brain injury. Front. Hum. Neurosci. 7, 1–11.

Cortes, C., Vapnik, V., 1995. Support-vector networks. Mach. Learn. 20, 273–297.

Costafreda, S.G., Chu, C., Ashburner, J., Fu, C.H.Y., 2009. Prognostic and diagnostic potential of the structural neuroanatomy of depression. PLoS One 4, e6353.

Dosenbach, N.U., Nardos, B., Cohen, A.L., Fair, D.A., Power, J.D., et al., 2010. Prediction of individual brain maturity using fMRI. Science 329, 1358–1361.

Fang, P., Zeng, L.L., Shen, H., Wang, L., Li, B., Liu, L., Hu, D., 2012. Increased cortical–limbic anatomical network connectivity in major depression revealed by diffusion tensor imaging. PLoS One 7, e45972.

Feng, Y., Abney, T.M., Okamoto, R.J., Pless, R.B., Genin, G.M., Bayly, P.V., 2010. Relative brain displacement and deformation during constrained mild frontal head impact. J. R. Soc. Interface 7, 1677–1688.

Gioia, G.A., Kenworthy, L., Isquith, P.K., 2010. Executive function in the real world: BRIEF lessons from Mark Ylvisaker. J. Head Trauma Rehabil. 25, 433–439.

Goh, S.Y.M., Irimia, A., Torgerson, C.M., Horn, J.D.V., 2014. Neuroinformatics challenges to the structural, connectomic, functional, and electrophysiological multimodal imaging of human traumatic brain injury. Front. Neuroinformatics 8, 1–12.

Guyon, I., Elisseeff, A., 2003. An introduction to variable and feature selection. J. Mach. Learn. Res. 3, 1157–1182.

Guyon, I., Weston, J., Barnhill, S., Vapnik, V., 2002. Gene selection for cancer classification using support vector machines. Mach. Learn. 46, 389–422.

Hammoud, K., Wasserman, B., 2002. Diffuse axonal injuries: a pathophysiology and imaging. Neuroimaging Clin. N. Am. 12, 205–216.

Hastie, T., Tibshirani, R., Friedman, J., 2001. The Elements of Statistical Learning. Springer.

Huisman, T., Schwamm, L., Schaefer, P., Koroshetz, W., Shetty-Alva, N., Ozsunar, Y., Wu, O., Sorensen, A., 2004. Diffusion tensor imaging as a potential biomarker of white matter in diffuse axonal injury. Am. J. Neuroradiol. 25, 370–376.

Inglese, M., Makani, S., Johnson, G., Cohen, B.A., Silver, J.A., Gonen, O., Grossman, R.I., 2005. Diffuse axonal injury in mild traumatic brain injury: a diffusion tensor imaging study. J. Neurosurg. 103, 298–303.

Irimia, A., Chambers, M.C., Torgerson, C.M., Filippou, M., Hovda, D.A., Alger, J.R., Gerig, G., Toga, A.W., Vespa, P.M., Kikinis, R., Horn, J.D.V., 2012a. a. Patient-tailored connectomics visualization for the assessment of white matter atrophy in traumatic brain injury. Front. Neurol. 3, 10.

Irimia, A., Wang, B., Aylward, S.R., Prastawa, M., Pace, D.F., Gerig, G., et al., 2012b. b. Neuroimaging of structural pathology and connectomics in traumatic brain injury: toward personalized outcome prediction. Neuroimage Clin. 1, 1–17.

Iverson, G.L., Lovell, M.R., Smith, S., Franzen, M.D., 2000. Prevalence of abnormal CT-scans following mild head injury. Brain Inj. 14, 1057–1061.

Jenkinson, M., 2003. Fast, automated, N-dimensional phase-unwrapping algorithm. Magn. Reson. Med. 49, 193–197.

Jenkinson, M., 2004. Improving the registration of B0-distorted EPI images using calculated cost function weights. Tenth Annual Meeting Of The Organization For Human Brain Mapping (pp. 1–1).

Jenkinson, M., Beckmann, C., Behrens, T., Woolrich, M., Smith, S., 2012. FSL. Neuroimage 62, 782–790.

Johnson, V.E., Stewart, W., Smith, D.H., 2013. Axonal pathology in traumatic brain injury. Exp. Neurol. 246, 35–43.

Jolliffe, I.T., 2002. Principal Component Analysis. second ed. Springer-Verlag, New York.

Jones, D.K., Horsfield, M.A., Simmons, A., 1999. Optimal strategies for measuring diffusion in anisotropic systems by magnetic resonance imaging. Magn. Reson. Med. 42, 515–525.

Kasahara, K., Hashimoto, K., Abo, M., Senoo, A., 2012. Voxel- and atlas-based analysis of diffusion tensor imaging may reveal focal axonal injuries in mild traumatic brain injury — comparison with diffuse axonal injury. Magn. Reson. Imaging 30, 496–505.

Kinnunen, K.M., Greenwood, R., Powell, J.H., Leech, R., Hawkins, P.C., Bonnelle, V., Patel, M.C., Counsell, S.J., Sharp, D.J., 2010. White matter damage and cognitive impairment after traumatic brain injury. Brain 134, 449–463.

Kraus, M.F., Susmaras, T., Caughlin, B.P., J Walker, C., Sweeney, J.A., Little, D.M., 2007. White matter integrity and cognition in chronic traumatic brain injury: a diffusion tensor imaging study. Brain 130, 2508–2519.

Kumar, R., Gupta, R.K., Husain, M., Chaudhry, C., Srivastava, A., Saksena, S., Rathore, R.K., 2009. Comparative evaluation of corpus callosum DTI metrics in acute mild and moderate traumatic brain injury: its correlation with neuropsychometric tests. Brain Inj. 23, 675–685.

Kurowski, B., Wade, S.L., Cecil, K.M., Walz, N.C., Yuan, W., Rajagopal, A., Holland, S.K., 2009. Correlation of diffusion tensor imaging with executive function measures after early childhood traumatic brain injury. J. Pediatr. Rehabil. Med. 2, 273–283.

Langs, G., Menze, B., Lashkari, D., Golland, P., 2011. Detecting stable distributed patterns of brain activation using Gini contrast. NeuroImage 56, 497–507.

Leemans, A., Jones, D., 2009. The b-matrix must be rotated when correcting for subject motion in DTI data. Magn. Reson. Med. 61, 1336–1349.

Lipton, M., Kim, N., Park, Y., Hulkower, M., Gardin, T., Shifteh, K., Kim, M., Zimmerman, M., Lipton, R., Branch, C., 2012. Robust detection of traumatic axonal injury in individual mild traumatic brain injury patients: intersubject variation, change over time and bidirectional changes in anisotropy. Brain Imaging Behav. 6, 329–342.

Liu, H., Motoda, H., 2007. Computational Methods of Feature Selection. Chapman and Hall/CRC Press.

Liu, M., Zeng, L.L., Shen, H., Liu, Z., Hu, D., 2012. Potential risk for healthy siblings to develop schizophrenia: evidence from pattern classification with whole-brain connectivity. NeuroReport 23, 265–269.

Love, R., Webb, W., 1992. Neurology for the Speech-Language Pathologist. Butterworth-Heinemann Limited (URL: https://books.google.com/books?id=2rlrAAAAMAAJ).

Lui, Y.W., Xue, Y., Kenul, D., Ge, Y., Grossman, R.I., Wang, Y., 2014. Classification algorithms using multiple MRI features in mild traumatic brain injury. Neurology 83, 1235–1240.

Matsushita, M., Hosoda, K., Naitoh, Y., Yamashita, H., Kohmura, E., 2011. Utility of diffusion tensor imaging in the acute stage of mild to moderate traumatic brain injury for detecting white matter lesions and predicting long-term cognitive function in adults. J. Neurosurg. 115, 130–139.

Meaney, D., Smith, D., 2011. Biomechanics of concussion. Clin. Sports Med. 30, 19–31.
Meythaler, J.M., Peduzzi, J.D., Eleftheriou, E., Novack, T.A., 2001. Current concepts: diffuse axonal injury-associated traumatic brain injury. Arch. Phys. Med. Rehabil. 82, 1461–1471.
Miles, L., Grossman, R.I., Johnson, G., Babb, J.S., Diller, L., Inglese, M., 2008. Short-term DTI predictors of cognitive dysfunction in mild traumatic brain injury. Brain Inj. 22, 115–122.
Modat, M., Ridgway, G.R., Taylor, Z.A., Lehmann, M., Barnes, J., Hawkes, D.J., Fox, N.C., Ourselin, S., 2010. Fast free-form deformation using graphics processing units. Comput. Methods Prog. Biomed. 98, 278–284.
Morris, D., Nossin-Manor, R., Taylor, M., Sled, J., 2011. Preterm neonatal diffusion processing using detection and replacement of outliers prior to resampling. Magn. Reson. Med. 66, 92–101.
Niogi, S., Mukherjee, P., 2010. Diffusion tensor imaging of mild traumatic brain injury. J. Head Trauma Rehabil. 25, 241–255.
Omalu, B., DeKosky, S., Minster, R., Kamboh, M., Wecht, C., 2005. Chronic traumatic encephalopathy in a National Football League player. Neurosurgery 57, 128–134.
Ourselin, S., Stefanescu, R., Pennec, X., 2002. Robust registration of multi-modal images: towards real-time clinical applications. Medical Image Computing and Computer-Assisted Intervention (MICCAI). volume 2489 of Lecture Notes in Computer Science, pp. 140–147.
Pandit, A.S., Expert, P., Lambiotte, R., Bonnelle, V., Leech, R., Turkheimer, F.E., et al., 2013. Traumatic brain injury impairs small-world topology. Neurology 80, 1826–1833.
Pannek, K., Mathias, J.L., Bigler, E.D., Brown, G., Taylor, J.D., Rose, S.E., 2010. An automated strategy for the delineation and parcellation of commissural pathways suitable for clinical populations utilising high angular resolution diffusion imaging tractography. NeuroImage 50, 1044–1053.
Pannek, K., Raffelt, D., Bell, C., Mathias, J.L., Rose, S.E., 2012a. a. Homor: higher order model outlier rejection for high b-value MR diffusion data. NeuroImage 63, 835–842.
Pannek, K., Guzzetta, A., Colditz, P.B., Rose, S.E., 2012b. b. Diffusion MRI of the neonate brain: acquisition, processing and analysis technique. Pediatr. Radiol. 42, 1169–1182.
Pearson, K., 1901. On lines and planes of closest fit to systems of points in space. Philos. Mag. 2, 559–572.
Povlishock, J.T., Katz, D.I., 2005. Update of neuropathology and neurological recovery after traumatic brain injury (review). J. Head Trauma Rehabil. 20, 76–79.
Robinson, E.C., Hammers, A., Ericsson, A., Edwards, A.D., Rueckert, D., 2010. Identifying population differences in whole-brain structural networks: a machine learning approach. NeuroImage 50, 910–919.
Rohde, G., Barnett, A., Basser, P., Marenco, S., Pierpaoli, C., 2004. Comprehensive approach for correction of motion and distortion in diffusion-weighted MRI. Magn. Reson. Med. 51, 103–114.
Rose, S., Pannek, K., Bell, C., Baumann, F., Hutchinson, N., Coulthard, A., McCombe, P., Henderson, R., 2012. Direct evidence of intra- and interhemispheric corticomotor network degeneration in amyotrophic lateral sclerosis: an automated MRI structural connectivity study. NeuroImage 59, 2661–2669.
Rosenbaum, S.B., Lipton, M.L., 2012. Embracing chaos: the scope and importance of clinical and pathological heterogeneity in mTBI. Brain Imaging Behav. 6, 255–282.
Sanchez, C., Richards, J., Almli, C., 2012. Age-specific MRI templates for pediatric neuroimaging. Dev. Neuropsychol. 37, 379–399.
Shenton, M., Hamoda, H., Schneiderman, J., Bouix, S., Pasternak, O., Rathi, Y., Vu, M., Purohit, M.P., Helmer, K., Koerte, I., Lin, A., Westin, C., Kikinis, R., Kubicki, M., Stern, R., Zafonte, R., 2012. A review of magnetic resonance imaging and diffusion tensor imaging findings in mild traumatic brain injury. Brain Imaging Behav. 6, 137–192.
Sled, J., Zijdenbos, A., Evans, A., 1998. A nonparametric method for automatic correction of intensity nonuniformity in MRI data. IEEE Trans. Med. Imaging 17, 87–97.
Smith, R., Tournier, J.D., Calamante, F., Connelly, A., 2012. Anatomically-constrained tractography: improved diffusion MRI streamlines tractography through effective use of anatomical information. NeuroImage 63, 1924–1938.
Smith, R., Tournier, J.D., Calamante, F., Connelly, A., 2013. SIFT: spherical-deconvolution informed filtering of tractograms. NeuroImage 67, 298–312.
Smith, R., Tournier, J.D., Calamante, F., Connelly, A., 2015. The effects of SIFT on the reproducibility and biological accuracy of the structural connectome. NeuroImage 104, 253–265.
Sugiyama, K., Kondo, T., Suzukamo, Y., Oouchida, Y., Sato, M., Watanabe, H., Izumi, S.I., 2013. Clinical utility of diffusion tensor imaging and fibre tractography for evaluating diffuse axonal injury with hemiparesis. Case Reports in Medicine, pp. 1–5.
Taber, K., Hurley, R., 2013. Update on mild traumatic brain injury: neuropathology and structural imaging. J. Neuropsychiatry Clin. Neurosci. 25, 1–5.
Tang, J., Alelyani, S., Liu, H., 2014. Data classification: algorithms and applications. CRC Press. chapter Feature Selection for Classification: A Review, pp. 1–33.
Tournier, J.D., Calamante, F., Gadian, D.G., Connelly, A., 2004. Direct estimation of the fiber orientation density function from diffusion-weighted MRI data using spherical deconvolution. NeuroImage 23, 1176–1185.
Tournier, J.D., Calamante, F., Connelly, A., 2007. Robust determination of the fibre orientation distribution in diffusion MRI: non-negativity constrained super-resolved spherical deconvolution. NeuroImage 35, 1459–1472.
Tournier, J.D., Calamante, F., Connelly, A., 2012. MRtrix: diffusion tractography in crossing fiber regions. Int. J. Imaging Syst. Technol. 22, 53–66.
Van Horn, J.D., Irimia, A., Torgerson, C.M., Chambers, M.C., Kikinis, R., Toga, A.W., 2012. Mapping connectivity damage in the case of phineas gage. PLoS One 7, e37454.
van Leemput, K., Maes, F., Vandermeulen, D., Suetens, P., 1999. Automated model-based tissue classification of MR images of the brain. IEEE Trans. Med. Imaging 18, 897–908.
Vapnik, V., Chervonekis, A., 1964. A note on one class of perceptrons. Autom. Remote. Control. 25.
Vapnik, V., Lerner, A., 1963. Pattern recognition using generalized portrait method. Autom. Remote. Control. 24.
Wada, T., Asano, Y., Shinoda, J., 2012. Decreased fractional anisotropy evaluated using tract-based spatial statistics and correlated with cognitive dysfunction in patients with mild traumatic brain injury in the chronic stage. Brain 33, 2117–2122.
Wang, J.Y., Bakhadirov, K., Devous Sr., M.D., Abdi, H., McColl, R., Moore, C., de la Plata, C.D.M., Ding, K., Whittemore, A., Babcock, E., Rickbeil, T., Dobervich, J., Kroll, D., Dao, B., Mohindra, N., Madden, C.J., Diaz-Arrastia, R., 2008. Diffusion tensor tractography of traumatic diffuse axonal injury. Arch. Neurol. 65, 619–626.
Wang, L., Shen, H., Tang, F., Zang, Y., Hu, D., 2012. Combined structural and resting-state functional MRI analysis of sexual dimorphism in the young adult human brain: an MVPA approach. NeuroImage 61, 931–940.
Wilde, E.A., Chu, Z., Bigler, E.D., et al., 2006. Diffusion tensor imaging in the corpus callosum in children after moderate to severe traumatic brain injury. J. Neurotrauma 23, 1412–1426.
Xu, J., Rasmussen, I.A., Lagopoulos, J., Haberg, A., 2007. Diffuse axonal injury in severe traumatic brain injury visualized using high-resolution diffusion tensor imaging. J. Neurotrauma 24, 753–765.
Yeh, P.H., Oakes, T.R., Riedy, G., 2012. Diffusion tensor imaging and its application to traumatic brain injury: basic principles and recent advances. Open J. Med. Images 2, 137–161.
Zalesky, A., Fornito, A., Bullmore, E.T., 2010. Network-based statistic: identifying differences in brain networks. NeuroImage 53, 1197–1207.
Ziv, E., Tymofiyeva, O., Ferriero, D.M., Barkovich, A.J., Hess, C.P., Xu, D., 2013. A machine learning approach to automated structural network analysis: application to neonatal encephalopathy. PLoS One 8, e78824.